Supplementary Materials

Superoxide Radical Formed on the TiO_2 Surface Produced from $Ti(OiPr)_4$ Exposed to H_2O_2/KOH

Rimma I. Samoilova [1] • Sergei A. Dikanov [2]

[1] Voevodsky Institute of Chemical Kinetics and Combustion, Russian Academy of Sciences, Novosibirsk 630090, Russian Federation
[2] Department of Veterinary Clinical Medicine, University of Illinois at Urbana-Champaign, Urbana, Illinois 61801, USA

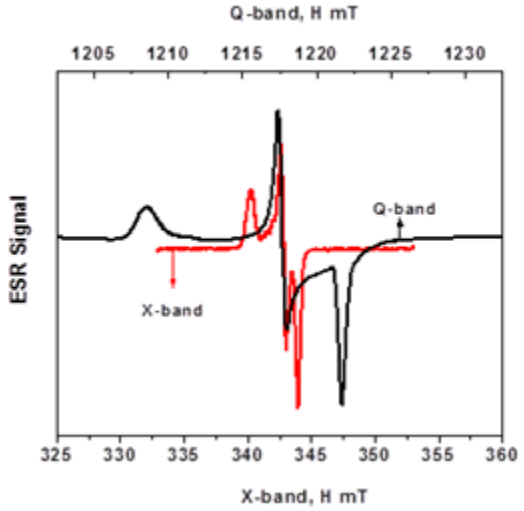

Figure S1. X- and Q-band EPR spectra of superoxide radical in sample **I** obtained as a first derivative of field sweep two-pulse ESE patterns. Experimental parameters: $\pi/2$ and π pulse length 100 and 200 ns, time between first and second pulses τ = 400 ns, microwave frequency 9.6352 GHz (X-band, red) and 34.1914 GHz (Q-band, black), and temperature 90 K. Adapted by permission from Copyright Clearance Center: Springer Nature, Samoilova *et al*. [S1]. Copyright 2022.

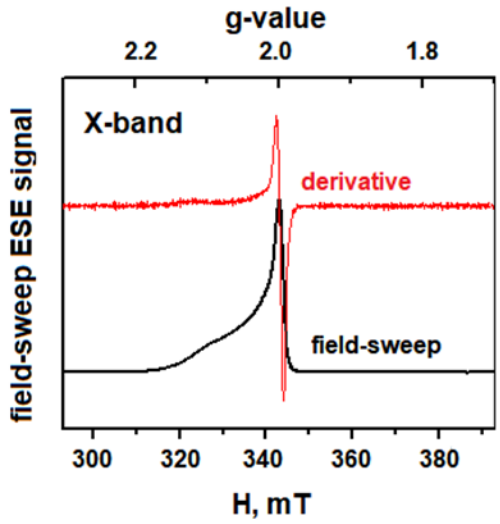

Figure S2. X-band two-pulse ESE field-swept spectrum and its first derivative of the TiO_2 surface produced from $Ti(OiPr)_4$ exposed to H_2O_2/KOH. Microwave frequency is 9. 6149 GHz, length of $\pi/2$ pulse is 16 ns, time τ between first and second pulses is 200 ns, and temperature is 15 K.

Table S1. *g*-tensors assigned to $O_2^{\bullet-}$ radical in different TiO_2 samples.

Matrix	g_{zz}	g_{yy}	g_{xx}	Reference
$Ti(OiPr)_4/H_2O_2$	2.024	2.009	2.003	S2
TiO_2(rutile) 30 wt% H_2O_2 60 wt% H_2O_2	2.025[a,b] 2.021[b]	2.009 2.009	2.003 2.003	S3
Ti-anatase (H_2O_2-treated)	2.025	2.011	2.0034	S4
Ti gel prepared from metallic Ti powder and 10M H_2O_2	2.023 2.025 2.021	2.009 2.009 2.009	2.003 2.003 2.003	S5
$Ti(OiPr)_4/H_2O_2$	2.0227[c] 2.024[d]	2.0074 2008	2.0010 2.002	S1
TiO_2 (P25)	2.019 2.020 2.023 2.026	2.011 2.011 2.011 2.011	2.005 2.004 2.004 2.001	S6,S7
TiO_2 on porous Vycor glass	2.0268	2.0088	2.0036	S8
dehydrated Pt/TiO_2 photo-catalysts (PT-1 and PT-2)	2.021 2.022	2.008 2.007	2.000 2.001	S9
TiO_2 (Millennium PC500, mesoporous)	2.0288	2.009	2.0037	S10
dye-sensitized TiO_2	2.0253	2.009	2.0031	S11
reduced TiAlPO-5	2.023	2.010	2.003	S12

[a]30 wt% H_2O_2, [b]60 wt% H_2O_2, [c]Q-band, [d]X-band. Adapted by permission from Copyright Clearance Center: Springer Nature, Samoilova *et al*. [S1]. Copyright 2022.

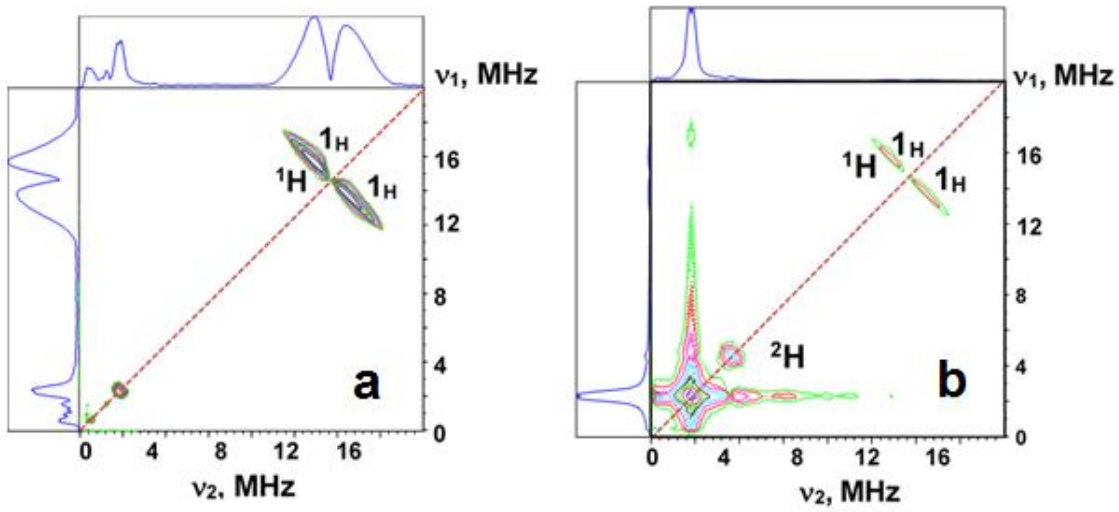

Figure S3. Contour representation of the HYSCORE spectra of superoxide radical in the sample **I** (a) and in the similar sample prepared using D_2O_2 (b). The time τ, between the first and the second microwave pulses, was 200 ns. The spectrum was obtained by FT of the 2D time domain patterns containing 256 × 256 points with a 16 ns step in t_1 and t_2, which are the intervals between the second and the third microwave pulses, and the third and the fourth microwave pulses, respectively. The microwave frequency was 9.635 GHz (a) and 9.6342 GHz (b), and the magnetic field was set to 342.9 mT (a) and 342.85 mT (b), and the temperature was 90 K. Adapted by permission from Copyright Clearance Center: Springer Nature, Samoilova *et al*. [S1]. Copyright 2022.

Section S1. Square frequency fitting of ^{1}H HYSCORE spectra and comparison with pulsed ENDOR data.

An estimate of the hyperfine couplings for the $\mathbf{1_H}$ cross-features in the samples **I** and **II** obtained using spectra from Figures S3 and 2. The coordinates (ν_1, ν_2) of arbitrary points along the proton ridges were measured and plotted as sets of values for ν_1^2 *vs.* ν_2^2 according to the Equation:

$$\nu_1 = (Q\nu_2^2 + G)^{1/2}, \qquad (1)$$

where $Q = (T+2a-4\nu_{1H})/(T+2a+4\nu_{1H})$ and $G = [2\nu_{1H}(4\nu_{1H}^2 - a^2 + 2T^2 - aT)]/(T+2a+4\nu_{1H})$ [S13]. This lineshape transforms into a straight line segment in ν_1^2 *vs.* ν_2^2 coordinates. It should be noted, however, that HYSCORE intensity at points ($\nu_{1\perp}$, $\nu_{2\perp}$) and ($\nu_{1\parallel}$, $\nu_{2\parallel}$), corresponding to orientations of the magnetic field along the $A_\perp$ and $A_\parallel$ principal directions of the hyperfine tensor, is equal to zero and is significantly suppressed at orientations around the principal directions [S14]. Therefore, in HYSCORE spectra, only the central part of the cross-ridge, which corresponds to orientations of the magnetic field substantially different from the principal directions, will possess observable intensity. The larger frequency of each point was arbitrarily selected as ν_1, and the smaller was selected as ν_2. The points have been fitted by linear regression (Figure S4) to give the slopes Q and intercepts G are shown in Table S2. Two sets of isotropic a and anisotropic T coupling defined by these Q and G are also included in this table.

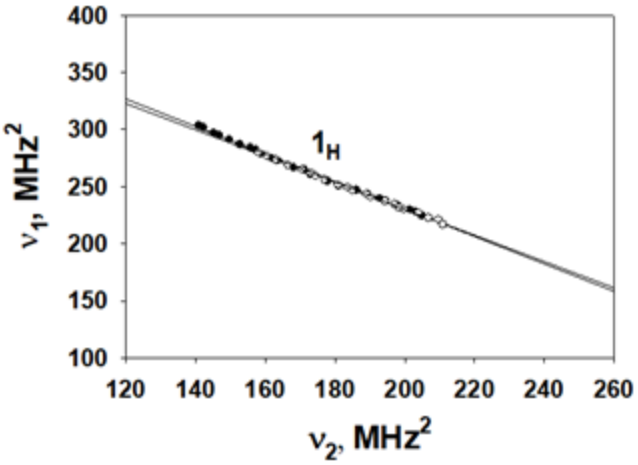

Figure S4. Plots of cross-ridges 1_H from HYSCORE spectra of superoxide radical in the sample **I** (Figure S4a, black circles) and in the similar sample prepared using D_2O_2 (Figure S4b, white circles) in the $(\nu_1)^2$ *vs*. $(\nu_2)^2$ coordinate system (see text for detailed explanations). The straight lines show the linear fit of plotted data points. Slope *Q* and intercept G for each fit are shown in Table S2. These values can then be used to obtain two possible solutions of isotropic (*a*) and anisotropic (*T*) couplings with the same value of |2*a*+T| and interchanged $A_\perp$= | *a* – T| and $A_\parallel$ = |*a*+2T|. Adapted by permission from Copyright Clearance Center: Springer Nature, Samoilova *et al*. [S1]. Copyright 2022.

Table S2. ^{1}H hyperfine tensor parameters determined from linear regressions of the cross-ridges.[a]

Sample		*Q*	*G*, MHz^2	a_1, MHz	a_2, MHz	*T*, MHz	Ref.
I (H_2O_2)	$\mathbf{1_H}$	-1.20 (0.014)	471.1 (2.4)	1.6	-3.8	2.2	S2
I (D_2O_2)	$\mathbf{1_H}$	-1.15 (0.013)	461.2 (2.4)	1.1	-3.0	1.9	S2
II	$\mathbf{1_H}$, $\mathbf{1_H}$**'**	-1.23 (0.02)	532.3 (2.3)	0.5	-6.5	7.0	This work

[a]Provided data define only the relative signs of *a* and *T*.
The positive sign of *T* is selected arbitrarily.

The HYSCORE analysis yields the presence of isotropic hyperfine coupling preferably of ~1 MHz. Its appearance likely arises from the incomplete suppression of the shoulders from ^{1}H intensive diagonal peak (Figure S3) and the heterogeneity of hyperfine interaction [S1].

Sample II. ^{1}H spectrum in Figure 2 clearly shows an additional feature $\mathbf{1_H}$**'**. During the analysis described above, we have found the slopes of the linear regression for the $\mathbf{1_H}$ and $\mathbf{1_H}$**'** lines possess an inverse relationship, i.e. Q(**1**) ~ 1/Q(**1'**). This means that the $\mathbf{1_H}$**'** peak is produced by the same proton(s) but belongs to the cross-feature with opposite assignment of the nuclear frequencies, i.e. (ν_2>ν_1) instead of (ν_1 >ν_2) [S14]. In other words, $\mathbf{1_H}$ and $\mathbf{1_H}$**'** are parts of the same cross-feature located on different sides relative to the diagonal of (++)-quadrant.

Figure S5 presents the plot where, the smaller coordinates for cross-peaks $\mathbf{1_H}$**'** were assigned to ν_1 and larger ones to ν_2, in contrast to peaks $\mathbf{1_H}$. In such a presentation, the points from $\mathbf{1_H}$ and $\mathbf{1_H}$**'** fit the linear regression well, thus confirming their assignment to the same

proton(s). The slope and intercept for the linear regression shown in Figure S5 are also presented in Table S2, together with two possible sets of (a,T) satisfying Eq.(1).

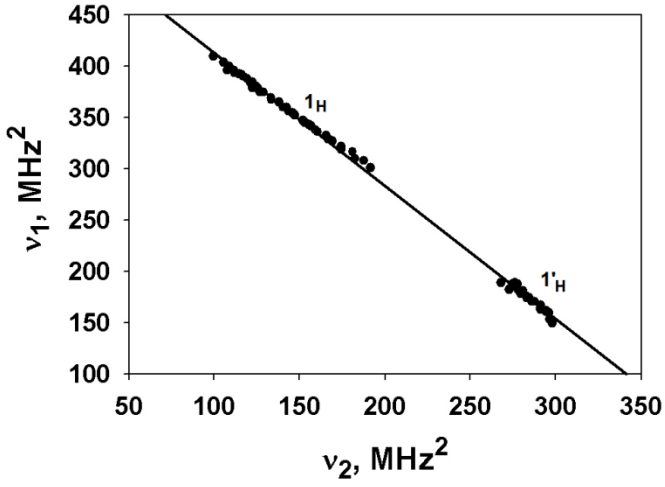

Figure S5. Plots of cross-ridges $\mathbf{1_H}$ and $\mathbf{1_H}$**'** from HYSCORE spectrum of superoxide radical in the sample **II** in the $(\nu_1)^2$ *vs.* $(\nu_2)^2$ coordinate system (see text for detailed explanations). The straight line shows the linear fit of plotted data points. Slope Q and intercept G for the fit are shown in Table S2. These values can then be used to obtain two possible solutions of isotropic (a) and anisotropic (T) couplings with the same value of $|2a+T|$ and interchanged $A_\perp = |a - T|$ and $A_\parallel = |a+2T|$.

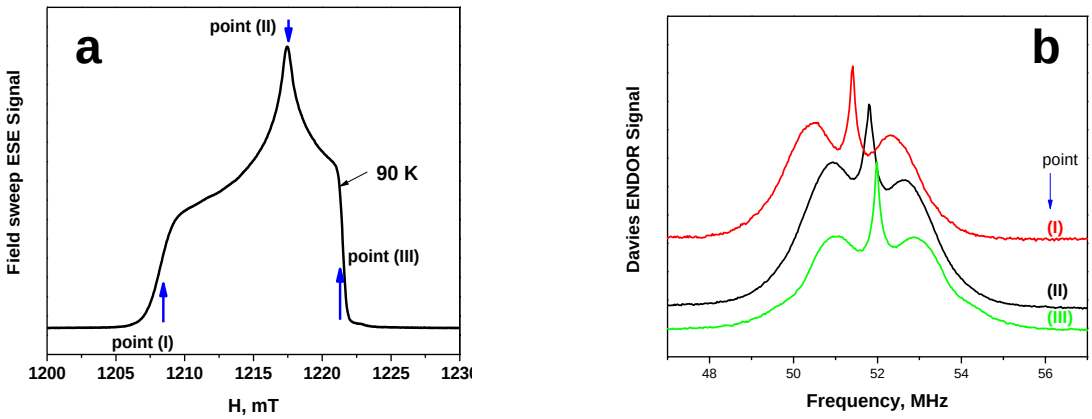

Figure S6. Q-band field-sweep 2-pulse ESE spectrum (a) and Q-band Davies ENDOR spectra (b) of the superoxide radical in sample **I**. The microwave frequency was 34.2198 GHz, $\pi/2$ pulse =100 ns, the magnetic field was set to 1208.0 mT (I), 1217.4 mT (II), 1221.5 mT (III), and the temperature was 90 K. Adapted by permission from Copyright Clearance Center: Springer Nature, Samoilova *et al*. [S1]. Copyright 2022.

For comparison, Q-band Davies ENDOR spectra collected at magnetic fields of the EPR spectrum corresponding to principal values of the g-tensor of the superoxide in the sample **I** (points I – III, Figure 6a) show the narrow matrix peak at the proton Zeeman frequency with two broad symmetrically located shoulders (Figure S6b). The splitting between the maxima of the shoulders in all three spectra is stable at 2.1 ± 0.1 MHz that is consistent with the value of

anisotropic coupling determined from the HYSCRE spectra. The maxima of the shoulders are defined by the frequencies of $\nu_{\pm} = |\nu_{1H} \pm T/2|$. ENDOR spectra (Figure S6b) of the sample **I** show two broad smooth lines without any additional features which could be assigned to parallel and perpendicular singularities of the hyperfine tensor from any individual proton. We suggested that these spectra are resulted from the bulk protons in the surrounding of the $O_2^{\bullet-}$ not involved in the direct interaction with the formation of the molecular bridge suitable for the electron spin density delocalization on *s*-orbital of proton. It is likely that the parameters determined from the analysis of the HYSCORE cross-ridges do not belong to specific interaction with the any selected proton(s), and nonzero isotropic coupling is resulted from the overlap of cross-ridges from protons with different anisotropic coupling. Similar conclusion could be made about the parameters obtained for the sample **I** in D_2O and for lines with the splitting ~1.5 MHz in ENDOR spectra of sample **II (**Figure S7**)**.

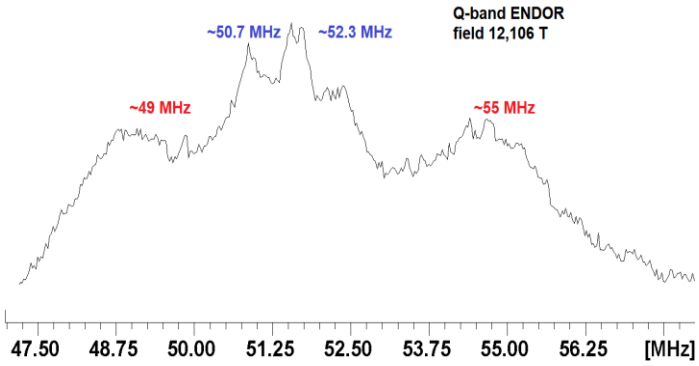

Figure S7. Q-band Davies ENDOR spectrum of the superoxide radical in sample **II.** The magnetic field was set to 12106 T ($g_{\perp}$), $\pi/2$ pulse =100 ns, RF pulse 12 μsec, temperature 15 K.

Analysis of the cross-ridges with the large deviation from the antidiagonal in square-frequency coordinates gives T=7.0 MHz a=-6.5 MHz or T=7.0 and a=0.5 MHz (Figure S5). These parameters define two values of $A_{\perp} = |a - T|$, i.e. |-6.5 - 7|=13 MHz and |0.5 - 7|=6.5 MHz. Last value is in a good agreement with the splitting ~ 6 MHz, observed in X and Q band spectra of the radical in sample **II**. The value of T=7.0 MHz is less than previously reported value of T~10 MHz for the superoxide in DMSO/H_2O solution [S15]. This result indicates probably the formation of a hydrogen bond with the paramagnetic center but the geometry of the H-bond and O…H distance supposed to be different in comparison with the cases of T~10 MHz.

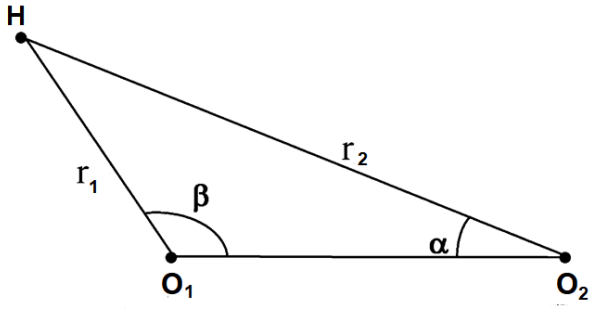

Figure S8. Definition of the distances and angles describing the location of the proton relative to O_1 and O_2 of the superoxide radical.

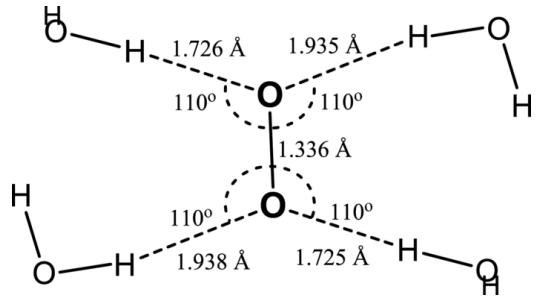

Figure S9. The UB3LYP/6-31 + G(d) structural model of $[O_2(H_2O)_4]^-$ is taken as an example from ref. S16. Several possible configurations are also discussed in refs. S17 and S18, which all predict the O−O bond length within the limit of 1.336 (±0.005) Å, and possibly contribute towards the site effect. Adapted by permission from Copyright Clearance Center: AIP Publishing, Janik *et al*. [S16]. Copyright 2013.

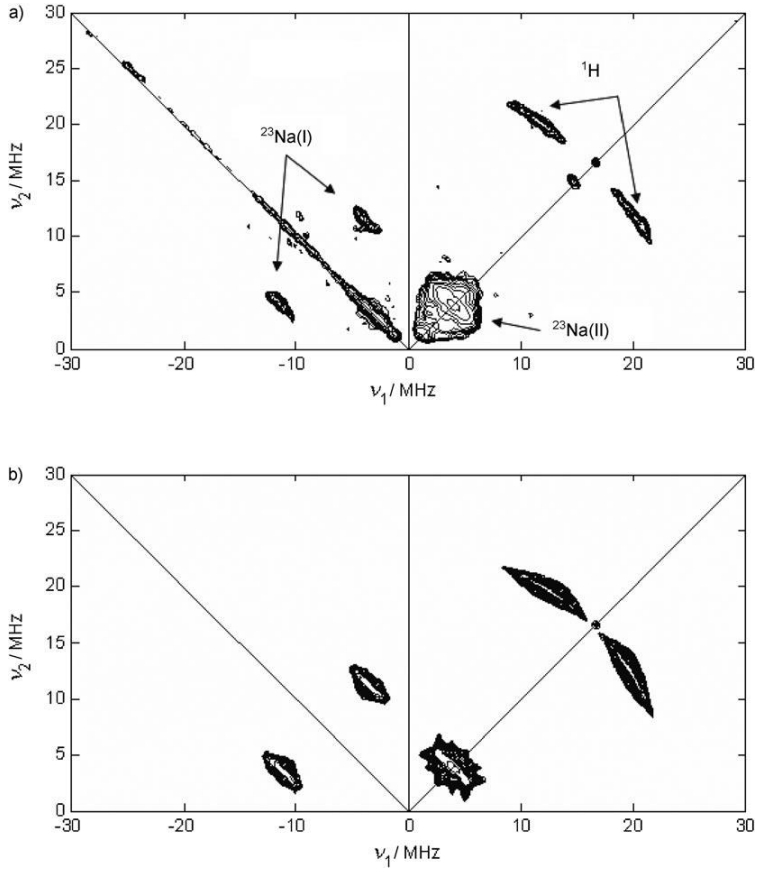

Figure S10. Experimental (top) and simulated (bottom) HYSCORE spectra of $O_2^{\bullet-}$ species on Na/MgO. The spectra were recorded at 10 K. Adapted by permission from Copyright Clearance Center: John Wiley and Sons, Napoli *et al*. [S19]. Copyright 2010.

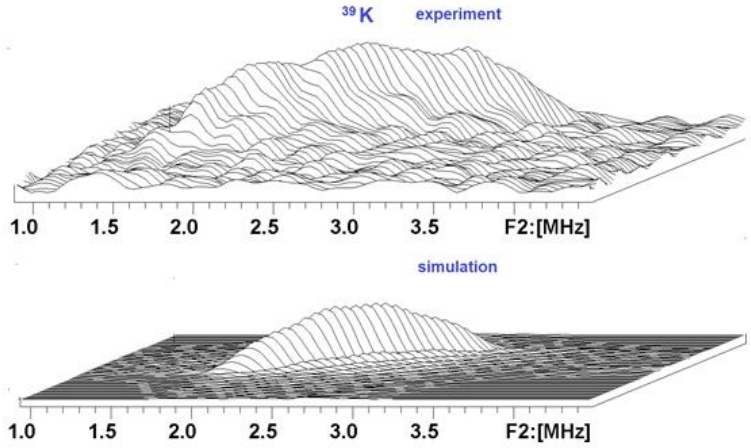

Figure S11. Stacked presentation of experimental ^{39}K HYSCORE spectrum of $O_2^{\bullet-}$ (top) and simulated (bottom) spectrum show qualitatively that an increased anisotropic coupling extends total length of the cross-ridge from ^{39}K and produces lineshape without well pronounced maxima around the diagonal.

References

S1**.** Samoilova, R.I.; Dikanov, S.A. Local environment of superoxide radical formed on the TiO_2 surface produced from $Ti(OiPr)_4$ exposed to H_2O_2. *Appl. Magn. Reson*. **2022,** *53*, 1089-1104.

S2**.** Dewkar, G.K.; Nikalje, M.D.; Sayyed, I.A.; Paraskar, A.S.; Jagtap, H.S.; Sudalai, A. *Angew. Chem. Int. Ed.* **2001**, *40*, 405-408.

S3. Antcliff, K. L., Murphy, D.M., Griffithsa, E., Giamello, E. The interaction of H_2O_2 with exchanged titanium oxide systems (TS-1, TiO2, [Ti]-APO-5, Ti-ZSM-5). *Phys. Chem. Chem. Phys*. **2003,** *5*, 4306–4316.

S4. Ramaswamy, V.; Awati, P.; Ramaswamy, A.V. Epoxidation of indene and cyclooctene on nanocrystalline anatase titania catalyst. *Top. Catal*. **2006**, *38*, 251-259.

S5. Tengvall, P.; Lundström, I.; Sjöqvist, L.; Elwing, H.; Bjursten, L. M. Titanium-hydrogen peroxide interaction: model studies of the influence of the inflammatory response on titanium implants. *Biomaterials* **1989**, *10*, 166-175.

S6. Green, J.; Carter, E.; Murphy, D. M. Interaction of molecular oxygen with oxygen vacancies on reduced TiO_2: Site specific blocking by probe molecules. *Chem. Phys. Lett*. **2009**, *477*, 340–344.

S7. Carter, E.; Carley, A. F.; Murphy, D. M. Evidence for O_2^- Radical Stabilization at Surface Oxygen Vacancies on Polycrystalline TiO_2. *J. Phys. Chem. C* **2007**, *111*, 10630-10638.

S8. Anpo, M.; Che, M.; Fubini, B.; Garrone, E.; Giamello, E.; Paganini, M.C. Generation of superoxide ions at oxide surfaces. *Top. Catal.* **1999**, *8*, 189–198.

S9. Liu, F., Feng, N., Wang, Q., Xu, J., Qi, G., Wang, W., Deng, F. Transfer Channel of Photoinduced Holes on a TiO_2 Surface As Revealed by Solid-State Nuclear Magnetic Resonance and Electron Spin Resonance Spectroscopy. *J. Am. Chem. Soc*. **2017**, *139*, 10020−10028.

S10. Rahemi, V.; Trashin, S.; Hafideddine, Z.; Meynen, V.; Van Doorslaer, S.; De Wael, K. Enzymatic sensor for phenols based on titanium dioxide generating surface confined ROS after treatment with H_2O_2. *Sensors and Actuators B: Chemical* **2019**, *283*, 343–348.

S11. Yu, J.; Chen, J.; Li, C.; Wang, X.; Zhang, B.; Ding, H. ESR Signal of Superoxide Radical Anion Adsorbed on TiO_2 Generated at Room Temperature. *J. Phys. Chem. B* **2004**, *108*, 2781-2783.
S12. Maurelli, S., Vishnuvarthan, M., Berlier, G., Chiesa, M. NH_3 and O_2 interaction with tetrahedral Ti^{3+} ions isomorphously substituted in the framework of TiAlPO-5. A combined pulse EPR, pulse ENDOR, UV-Vis and FT-IR study. *Phys. Chem. Chem. Phys*. **2012**,*14*, 987-995.
S13. Dikanov, S.A.; Bowman, M.K. Cross-peak lineshape of two-dimensional ESEEM spectra in disordered *S*=1/2, *I*=1/2 spin system. *J. Magn. Reson., Ser. A*, **1995**, *116*, 125-128.
S14. Dikanov, S.A., Tyryshkin, A.M.; Bowman, M.K. Intensity of cross-peaks in HYSCORE spectra of *S*=1/2, *I*=1/2 spin systems. *J. Magn. Reson*. **144**, *228* (2000).
S15. Samoilova, R.I.; Crofts, A.R.; Dikanov, S.A. Reaction of Superoxide Radical with Quinone Molecules. *J. Phys. Chem. A* **2011**, *115*, 11589–11593.
S16. Janik, I.; Tripathi, G.N.R. The nature of the superoxide radical anion in water. *J. Chem. Phys*. **2013**, *139*, 014302.
S17. Antonchenko, V.Y.; Kryachko, E.S. Interaction of superoxide O_2^- with water hexamer clusters. *Chem. Phys.* **2006**, *327*, 485-493.
S18. Antonchenko, V.Y.; Kryachko, E.S. Structural, Energetic, and Spectroscopic Features of Lower Energy Complexes of Superoxide Hydrates $O_2^-(H_2O)_{1-4}$. *J. Phys. Chem. A* **2005**, *109*, 3052-3069.
S19. Napoli, F.; Chiesa, M.; Giamello, E.; Preda, G.; Di Valentin, C.; Pacchioni, G. Formation of Superoxo Species by Interaction of O_2 with Na Atoms Deposited on MgO Powders: A Combined Continuous-Wave EPR (CW-EPR), Hyperfine Sublevel Correlation (HYSCORE) and DFT Study. *Chem.—Eur. J*. **2010**, *16*, 6776–6785.